RADIATION RESEARCH 172, 226–233 (2009)
0033-7587/09 $15.00

DOI: 10.1667/RR1746.1

Early-Stage Evolution of the EPR Spectrum of Crystalline Sucrose at Room Temperature after High-Dose X Irradiation

H. Vrielinck,[a,1,2] H. De Cooman,[a,3] Y. Karakirova,[b] N. D. Yordanov[b] and F. Callens[a]

[a] *Ghent University, Department of Solid State Sciences, Krijgslaan 281 – S1, B-9000 Gent, Belgium; and* [b] *Bulgarian Academy of Sciences, Lab EPR, Institute of Catalysis, BU-1113 Sofia, Bulgaria*

Vrielinck, H., De Cooman, H., Karakirova, Y., Yordanov, N. D. and Callens, F. Early-Stage Evolution of the EPR Spectrum of Crystalline Sucrose at Room Temperature after High-Dose X Irradiation. *Radiat. Res.* 172, 226–233 (2009).

X irradiation of sucrose single crystals at room temperature leads to the production of stable radicals, which give rise to the dosimetric electron paramagnetic resonance (EPR) signal. In the first few hours after irradiation, however, the shape of the EPR spectrum changes drastically. Based on two-dimensional field-frequency electron nuclear double resonance (FF-ENDOR) measurements, we demonstrate that, after high-dose (~5 kGy) and high-dose-rate irradiation, several species with limited stability at room temperature are produced next to the stable radicals. For two of these species, the main characteristics could be determined. Analysis of the time evolution of the FF-ENDOR and room-temperature EPR spectra in the first few hours after irradiation leads to the conclusion that these meta-stable radicals mainly recombine into diamagnetic species, while transformation into stable radicals is at most a marginal process. © 2009 by Radiation Research Society

INTRODUCTION

In the past few decades, several studies have concentrated on understanding the composite nature of the electron paramagnetic resonance (EPR) spectrum of irradiated sucrose (*1–6*). Recent combined electron magnetic resonance and density functional theory (DFT) research in our laboratory led to the structural identification of the stable radicals in X-irradiated sucrose, which are responsible for the major part (>80%) of the dosimetric EPR signal (*5, 6*). The T1 radical was identified as a C2′ centered radical in the fructose ring (*6*) and the T2/T3 radicals were shown to be two conformations of a C1 centered radical in the glucose unit (*5*). The formation of both types of stable radicals involves the cleavage of the glycosidic bond and the formation of a carbonyl group on the carbon next to the one with the main spin density. Because of this success, sucrose appears to be the ideal model system to study the reaction mechanisms that lead to the formation of these stable radicals. Primary radical formation and the evolution into stable radiation products are also relevant in the context of studies of radiation damage to DNA, where sugar radicals are expected to play an important role (*7*).

Several previous studies dealing with natural cane or beet sugar as well as its main component, sucrose, and concentrating on low (cGy) or high (~10 kGy) radiation doses have reported that the EPR spectrum of X-irradiated sucrose undergoes significant changes in the first hours up to several weeks after irradiation [see e.g. refs. (*8–10*)]. Therefore, in both structural and dosimetric studies of irradiated sugar, EPR spectra are usually only recorded at least 1 day after irradiation. In this study, we examined the spectrum immediately after high-dose irradiation at room temperature and its evolution during the first few hours toward its stable form. The primary aim was to investigate whether these spectral changes provide information about the mechanism of formation of the stable radicals.

MATERIALS AND METHODS

Sucrose was purchased from Aldrich, and small pieces were polished to fit Q-band (34 GHz) EPR/electron nuclear double resonance (ENDOR) sample tubes (1.4 mm inner diameter) with the long axis parallel to the crystallographic ⟨b⟩ axis, i.e. the twofold screw symmetry axis of the crystal (monoclinic symmetry, $P2_1$). X irradiation was performed at room temperature for 5 min (at a dose rate estimated at 1 kGy/min) using a Philips W-anode tube at 60 kV and 40 mA. Q-band EPR and ENDOR measurements were performed at 80 K (liquid N_2 cooling) on a Bruker Elexsys E500 spectrometer equipped with an Oxford CF935 cryostat. The ENDOR spectra were measured in the range of 40–110 MHz, sweeping the magnetic field over the complete EPR spectrum range. These spectra are referred to as Field-Frequency ENDOR (FF-ENDOR) spectra.

For the time-dependence study (t = 0 corresponds to the start of the irradiation), the EPR spectra were recorded at room temperature, with a modulation amplitude of 0.1 mT and a total recording time for

[1] Postdoctoral Fellow of the Flemish Research Foundation (FWO-Vlaanderen).

[2] Address for correspondence: Ghent University, Dept. Solid State Sciences, Krijgslaan 281-S1, B-9000 Gent, Belgium; email: Henk.Vrielinck@UGent.be.

[3] Research Assistant of the Flemish Research Foundation (FWO-Vlaanderen).

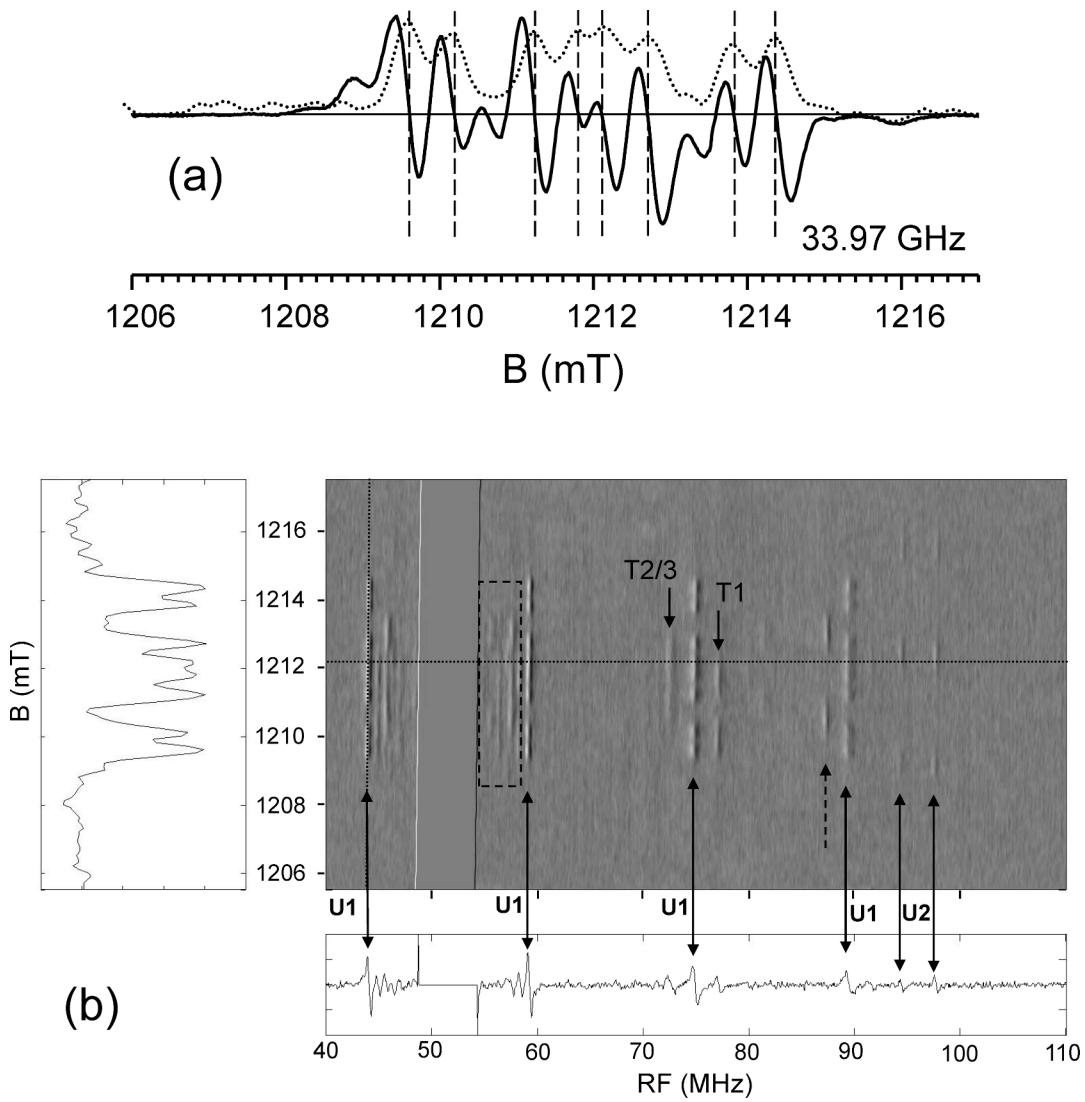

FIG. 1. Panel a: EPR spectrum of sucrose, 10 min after the start of the X irradiation (5 min at ~1 kGy/min) with B // ⟨a*⟩, recorded at 80 K and 33.97 GHz (full line), and compared with the ENDOR-induced EPR spectrum taken as the inclined vertical section (see text) in the FF-ENDOR spectrum (panel b) (dotted line). Panel b: FF-ENDOR spectrum (gray intensity scale, white: high positive, black: high negative). Underneath the FF-ENDOR spectrum, an ENDOR spectrum (horizontal section) is shown, and on the left an ENDOR-induced spectrum (inclined vertical section) is shown. Both sections are indicated by dotted lines in the FF-ENDOR spectrum. Signals of the stable (T1–3) and meta-stable that (U1–2) are indicated by solid arrows; the dashed arrow indicates an additional meta-stable radical that could not be characterized further.

each spectrum of 41 s. For these experiments the magnetic field was measured using a ER035 M NMR Gauss probe and calibrated with a standard DPPH field marker (g = 2.0036). All spectra were normalized to the same frequency (33.9935 GHz). Maximum likelihood factor analysis, as implemented in the statistical software package SPSS, was performed on the time series to determine the common spectral components. Essentially the same results were obtained using homemade maximum likelihood common factor analysis software, as described in ref. (*11*).

RESULTS AND DISCUSSION

FF-ENDOR Spectroscopy Results

The time evolution of the EPR spectrum that occurs at room temperature can be inhibited by cooling the sample. The shape of the EPR spectrum does not undergo drastic changes when cooled from room temperature to 80 K, except for minor changes in the relative line intensities, although at low temperature the microwave power has to be lowered to avoid saturation. Figure 1 shows the EPR and FF-ENDOR spectra at 80 K of a room-temperature X-irradiated sucrose single crystal approximately 10 min after the start of the irradiation (5 min irradiation time + 5 min transfer and cooling time) for a magnetic-field orientation close to the crystallographic ⟨a*⟩ axis. In spite of the multiline structure, the EPR spectrum appears to be fairly simple. The reason for this seeming simplicity is found in the FF-ENDOR spectrum, the general features of which will be described.

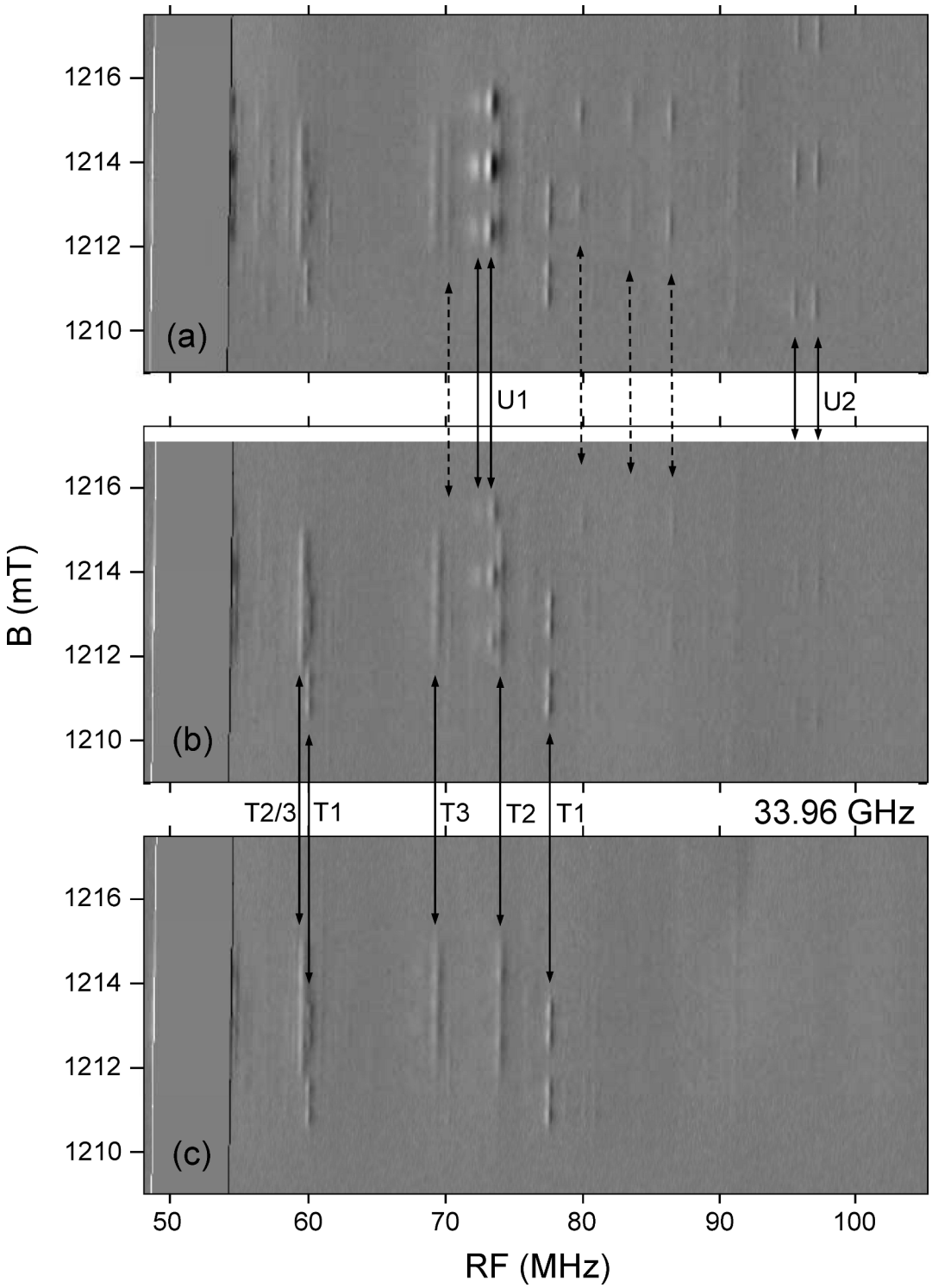

FIG. 2. Evolution of the FF-ENDOR spectrum at 80 K and 33.96 GHz of X-irradiated sucrose for a magnetic-field orientation in the {ca} plane, rotated ~30° away from the ⟨c⟩ axis (in the direction of ⟨a⟩). Panel a: 10 min after the start of the irradiation; panel b: after anneal to room temperature (total heating, annealing and recooling time ~3 h; panel c: after prolonged (~10 h) additional anneal at room temperature. Signals of the stable radicals (T1–3) and meta-stable radicals U1 and U2 are indicated by solid arrows. The dashed arrows indicate additional stable radicals that could not be characterized further.

Underneath the FF-ENDOR spectrum, a horizontal cross section, i.e. at constant field, is shown at the horizontal dotted line in the two-dimensional spectrum. Naturally, this corresponds to a regular, frequency-swept ENDOR spectrum at constant static field. Inclined vertical cross sections, as shown on the left of the FF-ENDOR spectrum and satisfying the field-frequency relationship,

$$S_{1D}(B) = S_{2D}\left(B, \nu_0 + \frac{g_N \mu_N (B - B_0)}{h}\right) \qquad (1)$$

(where S represents signal height, μ_B is the Bohr magneton, g_N the nuclear g factor, and h Planck's constant), correspond to ENDOR-induced EPR (EI-EPR) spectra for an ENDOR frequency ν_0 recorded at a static resonance field B_0. The second term in the second argument on the right-hand side of Eq. (1) accounts for the nuclear Zeeman energy shift the ENDOR transitions experienced when the magnetic-field strength is varied. These spectra are sometimes also referred to as field-swept ENDOR. As for paramagnetic centers with S = ½ interacting with nuclei with spin I = ½, all ENDOR transitions can be recorded at each EPR transition; the EI-EPR in principle reproduces the EPR spectrum of a certain (orientation of a) radical (*12*). In the FF-ENDOR spectrum, resonance spots of one (orientation of a particular) radical are situated on the grid formed by horizontal ENDOR and inclined vertical EI-EPR cross sections. Bearing this in mind, the FF-ENDOR spectrum in Fig. 1b appears to be dominated by a single radical characterized by three proton (^{1}H) hyperfine (HF) interactions, whose ENDOR frequencies are marked U1 in Fig. 1b (four ENDOR lines). Two more ENDOR transitions are expected to lie below 40 MHz. This leads to an EPR (and EI-EPR) spectrum consisting of a poorly resolved central quartet flanked by two split-off doublets. The dominance of this radical in the FF-ENDOR spectrum is also reflected in the total EPR spectrum (see Fig. 1a), hence its seeming simplicity. The FF-ENDOR spectrum, however, clearly shows that a variety of radicals are formed. One additional prominent radical is characterized by two large ^{1}H HF interactions (at ~95 and ~98 MHz) leading to a triplet EI-EPR pattern. These resonance frequencies are marked U2 in Fig. 1b. From the published spin Hamiltonian parameters in refs. (*4–6*), it is clear that neither U1 nor U2 can correspond to one of the stable radical species T1, T2 and T3, whose ENDOR frequency positions in the 70–80 MHz region are also marked in Fig 1b. At this particular magnetic-field orientation, the transitions of T2 and T3 approximately coincide. The lower-frequency transitions of these radicals occur in the overcrowded region marked with a dashed rectangle in Fig. 1b.

The occurrence of ENDOR transitions in expected frequency positions in itself is no proof for the presence of the stable radicals, because meta-stable radicals might have transitions in the same frequency region. Therefore, for several orientations, the FF-ENDOR spectra were also recorded after annealing the sample to room temperature, allowing the spectrum to evolve toward its stable shape. The assignments in Fig. 1b are based on such experiments, and the results for a magnetic-field orientation about 30° away from the ⟨c⟩ axis, where the ENDOR frequencies of T1, T2 and T3 are known to be clearly separated from one another (*4*), are shown in Fig. 2. The spectra were recorded 10 min after irradiation, after the sample was annealed to room temperature for a relatively short time (total heating and cooling time ~3 h), and after prolonged annealing (~10 h).

The evolution is clearly visible. In the spectrum immediately after irradiation (Fig. 2a), two ENDOR transitions of the dominant U1 radical nearly coincide at ~73 MHz. The triplet structure of its EI-EPR spectrum proves that these belong to two nearly equivalent but distinct HF interactions of the same radical. The transitions of the U2 radical, whose EI-EPR spectrum is a wider split triplet, appear again in the 95–98 MHz range (like in Fig. 1b). In Fig. 2c, only the transitions of the T1 and T2/T3 stable radicals have persisted. From the two meta-stable radicals described above, only faint traces are left. The comparison of Fig. 2a and c shows that in addition to U1 and U2, at least four more distinct meta-stable radical species (marked with dashed arrows) are produced by X irradiation at room temperature that have partially decayed in Fig. 2b and (almost) completely vanished in Fig. 2c. Finally, it should be noted that the transitions of the stable radicals are already present in Fig. 2a, i.e. immediately after irradiation, and that their intensity does not seem to be affected significantly by annealing.

As far as structural identification of the meta-stable radicals is concerned, little can be concluded from spectra at only a limited number of magnetic-field orientations in one rotation plane. Nonetheless, we can conclude that radical U1 has an α-^{1}H and one β-^{1}H coupling of intermediate strength, whereas U2 exhibits two large β-^{1}H couplings.

Time Dependence of the Room-Temperature EPR Spectrum

Figure 3a shows the field-corrected and frequency-normalized (see Materials and Methods section) first-derivative EPR spectra recorded with the magnetic field approximately parallel to the crystallographic ⟨c⟩ axis in a time series covering the first 6 h of evolution at room temperature. The first spectrum, recorded approximately 10 min after the start of the irradiation, and the last are shown in blue and red, respectively. In Fig. 3b, the field integrated spectra are displayed as a function of time on a color intensity scale (blue: 0, red: high). Both

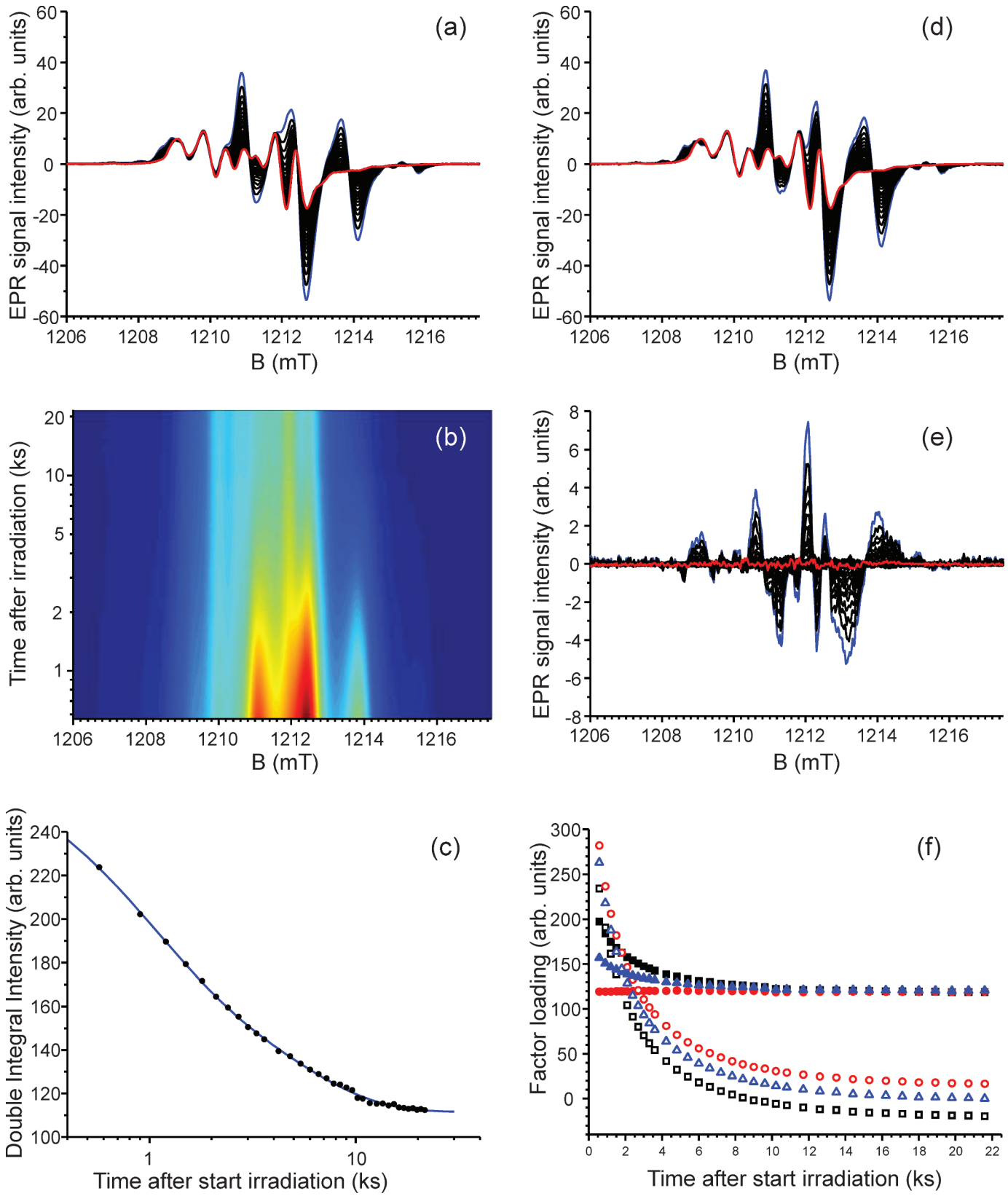

FIG. 3. Panel a: Time evolution of the room-temperature EPR spectrum of X-irradiated sucrose (~5 kGy) with B // ⟨c⟩, from 10 min (blue spectrum) to 6 h (red) after the start of the irradiation. The spectra are field-corrected (DPPH) and frequency-normalized (33.9935 GHz). Panel b: Color-scale (red: high, dark blue: zero) intensity plot of the integrated EPR spectra in panel a as a function of time after the start of the irradiation (logarithmic scale). Panel c: Total EPR intensity (double integration) as a function of time after irradiation (logarithmic scale). Filled circles represent experimental data points, and the full line shows the best-fit double exponential decay profile ($\tau_1 = 850$ s, $\tau_2 = 4700$ s). Panel d: Reconstruction of the

figures indicate that a component dominated by a broad-line triplet gradually vanishes from the spectrum and that the components in the final spectrum are already present immediately after irradiation. This viewpoint appears to be confirmed by the analysis of the time dependence of the total signal intensity, obtained by double integration of the spectra, as shown in Fig. 3c. The total intensity decays to less than half of its initial value and follows a double exponential time dependence, exhibiting a fast and a slow component with respective time constants $\tau_1 = 850$ s and $\tau_2 = 4700$ s. Other time dependences, e.g. single exponential or pair decay [$I(t) = A/(1 + t/\tau)$], lead to significantly worse agreement with experiment, in particular for the spectrum recorded 1 day after the start of the irradiation, not included in this series. The influence of the dose and dose rate on the concentration ratio of stable and unstable radicals was not checked, although we believe that these parameters may be very important.

Maximum likelihood factor analysis has been applied to determine the number of components that constitute the spectra. This analysis demonstrates that three (orthonormal) factor spectra are necessary to reproduce all spectra in the series. Each spectrum in the series (34 spectra) is perfectly reproduced as a linear combination of these three components. We refer to the weight coefficient of a certain factor in a particular spectrum as its loading. Two factor spectra are clearly dominant, bearing 89.60% and 10.35% of the total variance. Moreover, if the first 10 spectra are excluded from the analysis (~1 h), the series can be reproduced nearly perfectly with only two factor spectra. Figure 3d shows the reconstructed spectra using the latter two factors, and Fig. 3e shows the rest of the spectra. The latter appear to consist of a single component, exhibiting a single exponential decay with $\tau_r = 1200$ s. The loadings of the remaining two factors are represented by the filled and open squares in Fig. 3f. The factor spectra themselves are displayed in Fig. 4a and b. These are expected to be linear combinations of real component spectra (*11*). The time dependence of the loading of the second factor spectrum, evolving from positive to negative values, points to a decomposition into components without direct physical meaning. Because the factor spectra act as an orthonormal base for the spectra in the time series, any orthogonal transformation leads to a new base. Two of these possible transformations are discussed below.

Both the FF-ENDOR and time-dependent EPR results indicate that a decomposition in a time-independent and a time-decaying component may have physical relevance. Therefore, an orthogonal transformation was first sought that leaves the loading of one of the base spectra independent of time (~2% maximum deviation). The component loadings are displayed in Fig. 3f as filled and open circles, and the spectra are shown in Fig. 4c and d. The time dependence of the loading of the second base spectrum is well described by double exponential decay with constants $\tau_1 = 1000$ s and $\tau_2 = 4000$ s. Note that these decay constants are similar to those found in the decay of the total intensity (double integration) of the spectra. The second component does not decay to zero intensity, however. Hence a second transformation into possibly physical components is evident in which one of the components decays to zero. The results of this transformation are shown in Fig. 3f as filled and open triangles, with the component spectra in Fig. 4e and f. In Fig. 4g, the EPR spectrum recorded 1 day after irradiation is presented. As expected, this spectrum corresponds nearly perfectly to that in Fig. 4e. Subtracting the last spectrum in the time series from that recorded 1 h after irradiation (fast decay component eliminated) leads to a spectrum resembling very well the time-decaying base spectrum, as shown in Fig. 4h.

Inspection of the base spectra in Fig. 4a–f shows that, in spite of their differences, in each base they exhibit essentially the same main characteristics. The strongly decaying second components are dominated by a triplet, which, through comparison with the FF-ENDOR results, may be identified as radical U1. The structures on the low and high magnetic field side of the triplet can then be explained at least in part by the presence of U2. Simulations based on HF constants derived from the ENDOR spectrum for B // ⟨c⟩, using a plausible g value of 2.0032 for both radicals, are shown in Fig 4j and support this viewpoint. The first components, on the other hand, which have fairly constant loadings, should be dominated by contributions of T1 and T2/T3. The simulations of these three spectral components using the known HF tensors and g factors $g(T1) = 2.0064$ and $g(T2/3) = 2.0055$ in Fig 4i demonstrate that this is indeed the case. Hence the analysis of the time dependence of the EPR spectrum after irradiation indicates that the stable radicals are already present immediately after irradiation and that their concentration remains constant or experiences a slight decay. We may thus safely state that the dominant radicals in the vanishing component (among others U1 and U2) have no part in the reaction mechanism leading to the stable radicals.

The appearance of a third factor in the first hour after irradiation, with a decay constant similar to that of the

←

spectra in panel (first in blue, last in red) using two components found in maximum likelihood factor analysis on the time series, excluding the first 10 spectra. Panel e: Rest spectra after subtracting those in panel d from the spectra in panel a (first in blue, last in red). Panel f: Time dependence of the loading of the base spectra in Fig. 4. Filled and open squares represent the maximum likelihood factors in Fig. 4a and b; filled and open circles represent the base spectra after transformation that leaves one of the loadings independent of time in Fig. 4c and d; filled and open triangles represent the base spectra after transformation leading one of the component loadings to decay to zero in Fig. 4e and f.

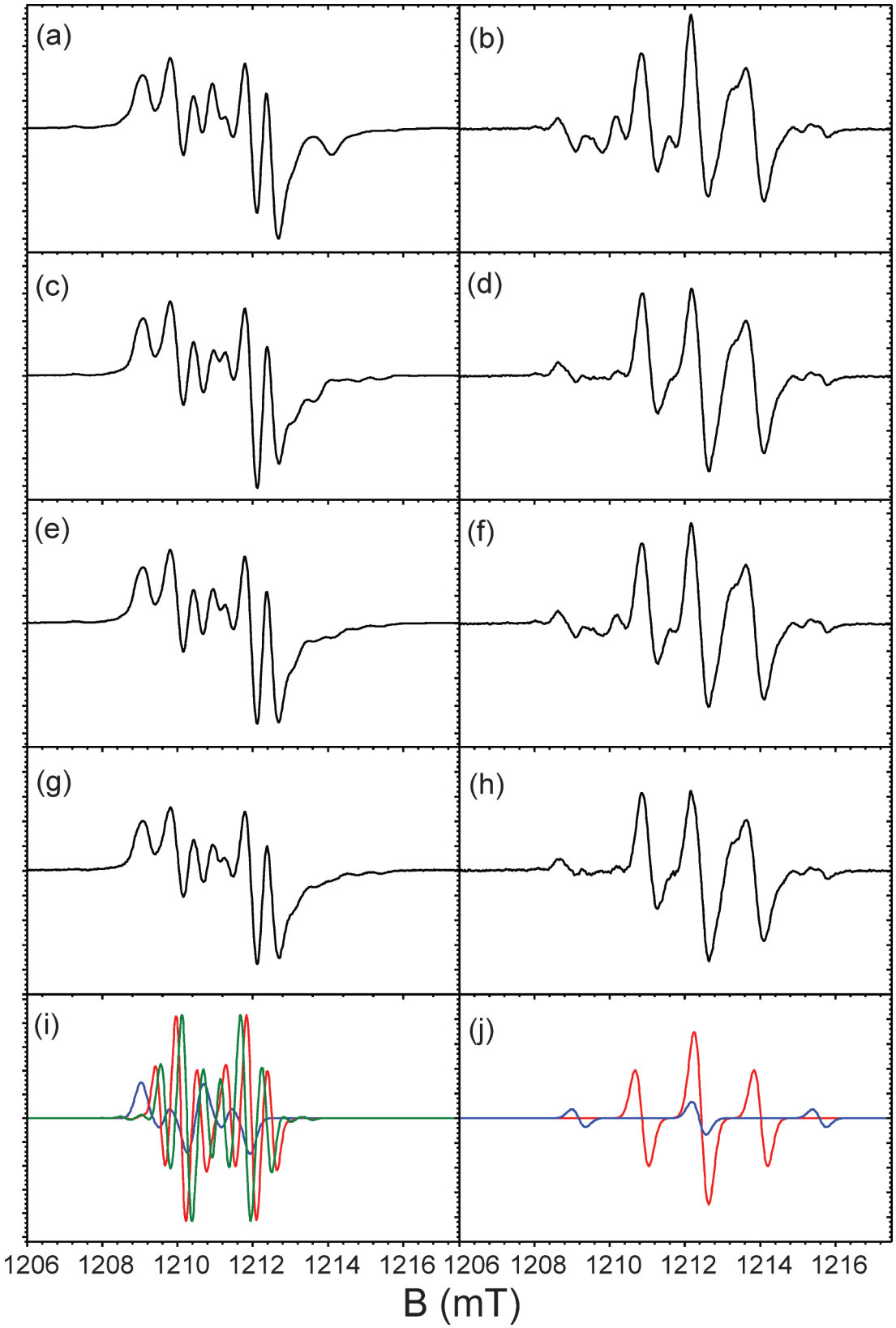

FIG. 4. Base spectra for decomposition of the time series. Panels a and b: As obtained from maximum likelihood factor analysis; panels c and d: after orthogonal base transformation making the loading for one of the base spectra independent of time; panels e and f; after orthogonal base transformation leading one of the component loadings to decay to zero. The spectra in panels b, d and f exhibit a much stronger time dependence than those in panels a, c and e (see loadings in Fig. 3e). Panel g: Spectrum recorded 1 day after the start of the irradiation. Panel h: Difference spectrum between the eleventh and the last spectra in the time series (Fig. 3). Panel i: Simulation of the T1 (blue), T2 (red) and T3 (green) stable spectrum components using their known (*4*) HF tensors and g(T1) = 2.0064 and g(T2/3) = 2.0055. Panel j: Simulation of the U1 (red) and U2 (blue) meta-stable spectrum components using HF parameters extracted from ENDOR spectra recorded with B // $\langle c \rangle$ and g(U1/2) = 2.0032.

fast component in the double exponential decay of the vanishing component, suggests that irradiation at room temperature also produces radicals with very limited stability. Due to their low abundance, it is difficult to establish whether these play an essential role in the radiation chemistry of the stable radicals, although even in the first hour after irradiation, no significant growth of the T1–3 components is observed. *Ex situ* irradiation at room temperature in any case seems inappropriate to study the structure and role of such very unstable radicals. EPR and ENDOR measurements on crystals irradiated at cryogenic temperatures will therefore be necessary to obtain insight into the radiation chemistry leading to the stable radicals in sucrose. Such experiments and their analyses are currently in progress, and the results will be reported in the near future.

Finally, we want to point out a few shortcomings of the analysis of the EPR spectrum's time dependence of the EPR spectrum as presented here. First, the decomposition method assumes that the spectral shape for a particular radical does not change with time, although changes, e.g. in line width, might occur as a result of the decrease in local radical concentration. This might lead to the discovery of additional factor spectra. Second, the effects of the finite recording time have not been taken into account. These are expected to distort the radical spectral components because the concentration of radicals decays during the scan. This is particularly important in the beginning of the time evolution, where fast decay components are present. Pulse EPR experiments allowing for shorter recording times (for essentially the same signal-to-noise ratio) might provide an important improvement in such experiments.

CONCLUSIONS

High-dose (~5 kGy) X irradiation at room temperature produces, next to the stable radicals T1 and T2/T3, several radical species with limited stability at room temperature, as seen using FF-ENDOR spectroscopy. The most prominent of those, labeled U1, is characterized by an α-proton coupling and a β-coupling with intermediate strength, whereas one of the secondary meta-stable radicals, labeled U2 shows two strong β-proton couplings. A detailed analysis of the time dependence of the EPR spectrum during the first 6 h after X irradiation leads to the conclusion that these meta-stable radicals decay without (or with at most very little) transformation into stable radicals. The study of their structure therefore is not expected to provide information on the processes of glycosidic bond cleavage and carbonyl formation, which characterize the stable radicals T1 and T2/T3. A study of radicals produced after low-temperature irradiation and their transformation as the temperature is increased, currently ongoing in our laboratory, will provide further information on the role of the U1 and U2 radicals in the radiation chemistry of sucrose and the possible implications for radiation damage in DNA. In view of their limited lifetime (~1 day), the meta-stable radicals reported here are not expected to influence dose assessments in sucrose EPR dosimetry, if, as usual, measurements are not performed earlier than a couple of days after exposure.

ACKNOWLEDGMENTS

H. Vrielinck and H. De Cooman acknowledge a postdoctoral fellowship and research assistant position, respectively, at the Flemish Research Foundation (FWO-Vlaanderen). This work was supported financially by the same institution and by a bilateral collaborative project VS.013.09N (Flanders – Bulgaria).

Received: February 10, 2009; accepted: April 3, 2009

REFERENCES

1. E. Sagstuen, A. Lund, O. Awaldelkartim, M. Lindgren and J. Westerling, Free radicals in X-irradiated single crystals of sucrose: a reexamination. *J. Chem. Phys.* **90**, 5584–5588 (1986).
2. G. Vanhaelewyn, J. Sadlo, F. Callens, W. Mondelaers, D. De Frenne and P. Matthys, A decomposition study of the EPR spectrum of irradiated sucrose. *Appl. Radiat. Isot.* **52**, 1221–1227 (2000).
3. E. R. Georgieva, L. Pardi, G. Jeschke, D. Gatteschi, L. Sorace and N. D. Yordanov, High-field/high-frequency EPR study on stable free radicals formed in sucrose by gamma-irradiation. *Free Radic. Res.* **40**, 553–563 (2006).
4. H. De Cooman, E. Pauwels, H. Vrielinck, A. Dimitrova, N. Yordanov, E. Sagstuen, M. Waroquier and F. Callens, Radiation-induced defects in sucrose single crystals, revisited: A combined electron magnetic resonance and density functional theory study. *Spectrochim. Acta A* **69**, 1372–1383 (2008).
5. H. De Cooman, E. Pauwels, H. Vrielinck, E. Sagstuen, F. Callens and M. Waroquier, Identification and conformational study of stable radiation-induced defects in sucrose single crystals using density functional theory calculations of electron magnetic resonance parameters. *J. Phys. Chem. B* **112**, 7298–7307 (2008).
6. H. De Cooman, E. Pauwels, H. Vrielinck, S. Van Doorslaer, F. Callens and M. Waroquier, ENDOR and HYSCORE analysis and DFT-assisted identification of the third major stable radical in sucrose single crystals X-irradiated at room temperature. *Phys. Chem. Chem. Phys.* **11**, 1105–1114 (2009).
7. W. A. Bernhard and D. M. Close, DNA damage dictates the biological consequences of ionizing irradiation: The chemical pathways. In *Charged Particle and Photon Interactions with Matter: Chemical, Physicochemical, and Biological Consequences with Applications* (A. Mozumder and and Y. Hatano, Eds.), pp. 431–470. Marcel Dekker, New York, 2003.
8. P. Fattibene, T. L. Duckworth and M. F. Desrosiers, Critical evaluation of the sugar-EPR dosimetry system. *Appl. Radiat. Isot.* **47**, 1375–1379 (1996).
9. M. Desrosiers and S. Wadley, Time-dependence of radiation-induced EPR signal in sucrose. *Radiat. Prot. Dosim.* **118**, 479–481 (2006).
10. N. D. Yordanov and E. Georgieva, EPR and UV spectral study of gamma-irradiated white and burned sugar, fructose and glucose. *Spectrochim. Acta A* **60**, 1307–1314 (2004).
11. P. Moens, P. De Volder, P. Hoogewijs, F. Callens and R. Verbeeck, Maximum-Likelihood Common-Factor Analysis as a powerful tool in decomposing multicomponent EPR powder spectra. *J. Magn. Reson. A* **101**, 1–15 (1993).
12. N. M. Atherton, *Principles of Electron Spin Resonance*. Ellis Horwood–Prentice Hall, New York, 1993.